*Progress In Electromagnetics Research M, Vol. 120, 113–122, 2023*

# Design of a Hollow Dielectric Loading for Wideband Gain Enhancement of a Horn Antenna

**Al-Moatasem Al-Hinaai[1, *], Anthony N. Caruso[1, 2], Roy C. Allen[2], and Kalyan C. Durbhakula[2]**

**Abstract**—The far-field gain of commercial horn antennas primarily depends on aperture area and flare length. Traditionally, for every dBi of gain increment, the flare length should increase by 20% and the aperture area by 10%. External lens classes, such as gradient refractive index, concave, or Fresnel, are used to improve gain by $\leq$ 2 dBi, but at the cost of a volumetric increase by 75% in the range of 4.8–6 GHz. We propose a hollow dielectric loading (HDL) loaded in the flare section of the horn antenna. The shape and position of the HDL are optimized using an evolutionary algorithm to obtain the maximum gain from a conical corrugated horn antenna (CCHA) at boresight. The optimized design yielded a total volume 40% smaller than traditional horn while achieving 3.5 dBi peak gain improvement in the operating frequency range. We also observed an improvement in the electric field by 24% while retaining parity in the impedance bandwidth. A 3D-printed prototype of the optimized CCHA and the HDL is fabricated and measured. The measured and simulated results demonstrated good agreement with a maximum difference of 4%.

## 1. INTRODUCTION

Corrugated conical horn antennas (CCHAs) are actively used in satellite communications, ground penetrating radar, reflectometry radar, and as a feed horn for dish reflector antennas due to their low side-lobe and cross-polarization levels [1–5]. Horn antennas provide wideband gain enhancement without increasing the aperture area significantly. They are valuable in space-limited applications and where antenna size is constrained. This ability is crucial for meeting the demands of modern wireless communication systems, allowing efficient communication across multiple frequency bands while remaining compact and cost-effective. Research has been carried out to enhance the directivity and therefore the gain of the horn antennas to communicate over farther distances without increasing the aperture area by approximately 10% for every unit value of dBi.

There are numerous geometry options and methods for enhancing the gain of the radiation pattern at the boresight [6–9]. Belen et al. proposed using multi-layer lenses for a horn antenna with five square-shaped layers of varying permittivity and thickness [6]. Asok et al. designed a half-cylinder dielectric load in the flared region of a double-ridge horn to improve its radiation performance and increase the gain bandwidth [7]. Other researchers designed a dielectric loading structure in front of a horn that matches the aperture area [8]. Additionally, a technique involving a cylinder pyramid of the aperture has been proposed to enhance the gain of a double-ridge conical horn [9]. While the designs proposed in [6–9] demonstrated an average gain enhancement of 2 dBi, they are heavy, bulky, and expensive to fabricate. A solid dielectric loading in front of the aperture exhibits some level of loss or attenuation, reduces overall antenna efficiency, and can result in a narrower frequency range as well as increased sidelobes and spillover.

*Received 28 July 2023, Accepted 16 October 2023, Scheduled 29 October 2023*

* Corresponding author: Al-Moatasem Al-Hinaai (aawvp@mail.umkc.edu).

[1] School of Science and Engineering, University of Missouri-Kansas City, Kansas City, MO 64110, USA. [2] Missouri Institute for Defense and Energy, University of Missouri-Kansas City, Kansas City, MO 64110, USA.

A CCHA's aperture area and the flare length determine the antenna gain [10–12]. Increased aperture dimension results in higher CCHA gain, which rises to a maximum at the boresight and falls off due to beam splitting. The decrease in antenna gain stems from increasing cylindrical wave phase error as the aperture increases while the length remains the same [13–15]. We present a new loading design that improves the directivity and minimizes impedance reflections to the feed of the CCHA. The choice of appropriate dielectric geometry and relative permittivity also determines the shape of the radiation pattern, which in turn changes the directivity [16]. The hollow dielectric loading (HDL) allows the electromagnetic (EM) waves to move unimpeded and limits reflection to the waveguide resulting in minimal bandwidth change. The main advantages of CCHA are their improved radiation efficiency compared to a traditional horn antenna, increased directivity, better pattern control, improved impedance matching, and low side-lobe and cross-polarization levels [14, 15]. These features make CCHA an ideal choice for outdoor applications where other types of antennas may not be suitable [17–19].

We demonstrate the workings of an HDL by designing a 5.4 GHz center frequency CCHA, followed by simulations and measurements to confirm its effectiveness over state-of-the-art loading designs. The prototype showed increased antenna gain compared to the commercial CCHA.

## 2. HOLLOW DIELECTRIC LOADING DESIGN AND OPTIMIZATION

The modeling of the proposed design and the antenna is carried out using CST Studio Suite [20, 21]. The finite integration technique solver has been used to evaluate the scattering parameters, antenna gain, and radiation pattern of the standalone CCHA and in the presence of the HDL. Conventional parametric study encompasses a wide solution search space, demanding substantial computation and storage capacity, as well as considerable simulation time. To avoid uncertainty, we have used the evolutionary algorithm (EA) available within the CST studio suite, providing a nature-inspired optimization of the HDL design, aiming to minimize the overall HDL volume while maximizing antenna gain. All the necessary parameters for calculating the HDL's volume using (1) serve as inputs to the EA for optimization [22].

$$V = \frac{L_4\pi}{3}(R^2 + Rr + r^2 - S^2 - Ss - s^2) \tag{1}$$

where $L_4$ represents the hypotenuse of the HDL, $R$ the top outside radius of the HDL, and $r$ the bottom outside radius of the HDL. The thicknesses at the top and bottom are denoted by $S$ and $s$, respectively. Fig. 1 illustrates the design of both the CCHA and HDL, wherein their apertures are located at the

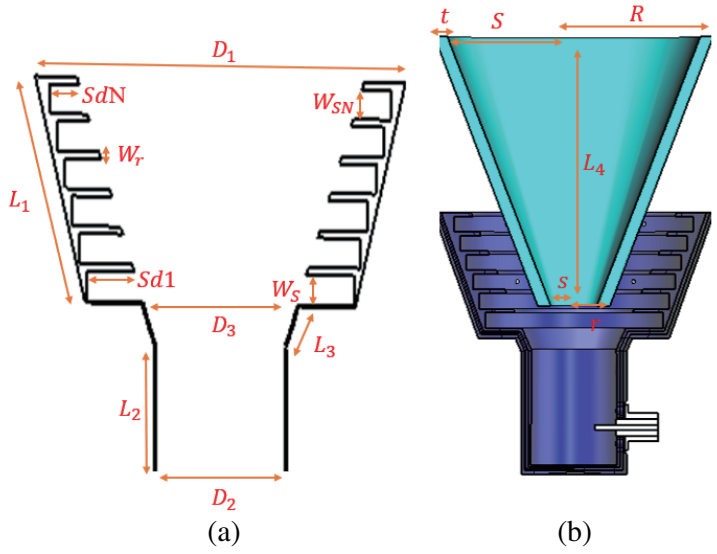


**Figure 1.** A cross-section view with relevant design variables of the (a) standalone CCHA, and (b) CCHA with HDL.

same position, and the entire HDL is situated inside the CCHA. Fig. 1(a) and Fig. 1(b) also show various variables associated with designing the CCHA and HDL, respectively.

The HDL parameters were optimized for high gain in the lowest volume using the Genetic Algorithm (GA). We have used a mutation rate of 60%. The GA was utilized for its effectiveness in achieving convergence quickly. The results from employing the GA and the best-fit curves to understand the behavior of HDL on antenna gain are presented in Fig. 2. Based on the findings, the gain increases as the GA iterations increase, but only up to approximately 150 iterations as shown in Fig. 2(a). Beyond that point, the increase in gain becomes minimal. Similarly, in Fig. 2(b), the volume exhibits an incremental pattern with the number of GA iterations. Fig. 2(c) shows that the gain and volume increase concurrently. A 3D scatter plot of volume, gain, and GA iterations is shown in Fig. 2(d), indicating that the gain and volume rise to a certain point as the GA iterations increase. The relationship between gain and volume is nonlinear, with the plot of gain versus volume showing a quadratic trend. The study uncovered insights into the optimal values of the HDL in the presence of the CCHA for achieving higher gain in a relatively small volume.

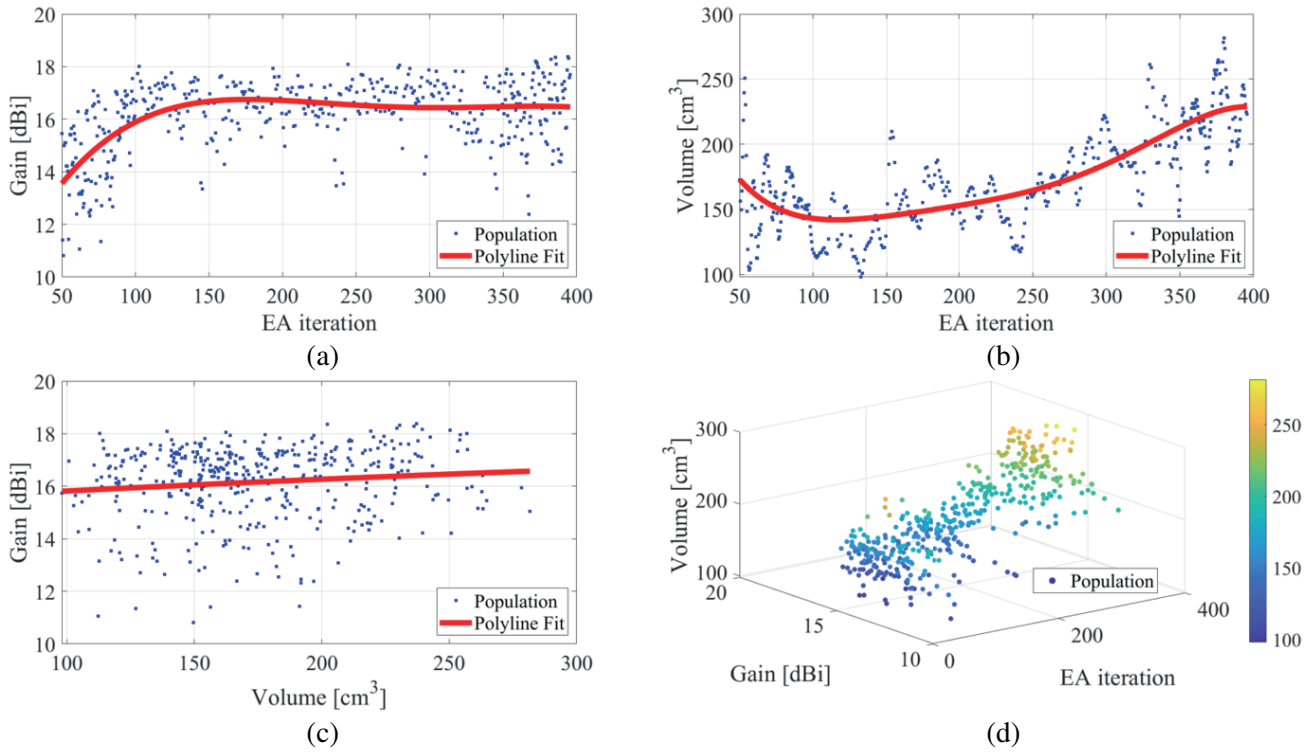


**Figure 2.** The optimal solution achieved by EA employed on the CCHA with HDL model: (a) EA iteration and the gain, (b) EA iteration and the volume, (c) volume and the gain, (d) 3D scatter plot between the EA iteration, the gain, and the volume.

## 3. ADDITIVE MANUFACTURING OF CCHA AND HDL

The main advantage of HDL over external lenses is that it avoids blocking the aperture core of the CCHA, resulting in reduced attenuation and improved overall antenna performance. By eliminating the obstruction caused by external lenses, HDL allows for better radiation efficiency and avoids potential signal loss, making it a favorable choice for enhancing gain and minimizing attenuation in the antenna system. The HDL consists of two open radii. One is located in the middle of the CCHA, while the other is situated by the aperture. The overall shape of the HDL corresponds to that of a cone, like the shape of the horn. The former should be sufficiently large for incoming radiation to pass through without reflecting off of the waveguide, while the latter must allow all signals to pass and focus the electric field.

The horn antenna and hollow dielectric were 3D-printed using polylactic acid (PLA) material in multiple parts. A standalone prototype of the hollow dielectric 3D-printed out of PLA is shown in Fig. 3(a). The CCHA was 3D-printed as a few different parts due to constraints in the printer's build volume. The conductive coating is applied to the surface of each printed object using silver as the raw material. Finally, the CCHA's metalized parts were assembled. Each part is equipped with alignment pins and snug-fit holes to ensure proper alignment during assembly. Fig. 3(b) shows the completed 3D-printed CCHA after the metal coating process. Fig. 3(b) also shows the hollow dielectric loaded into the 3D-printed and metalized CCHA. The traditional method of manufacturing an aluminum CCHA would result in a weight of 777 grams, while our 3D-printed CCHA method produces a weight of 320 grams, which is 40% lighter. An N-type connector was used on the CCHA, and the full prototype was experimentally verified to demonstrate the projected improvement. The measured results are compared against the simulated data.

(a) (b)

**Figure 3.** (a) 3D-printed HDL prototype. (b) 3D-printed HDL integrated with CCHA prototype.

## 4. RESULTS AND DISCUSSION

The performance of the CCHA antenna with and without HDL is simulated and experimentally verified. Table 1 shows the optimized CCHA and HDL design parameters for a center frequency of 5.4 GHz. The choice of 5.4 GHz as the center frequency is intended for testing the theory of the HDL's capability to enhance the gain of the horn antenna. The initial waveguide section of the CCHA is designed to radiate frequencies from 4.8 to 6 GHz. The simulation and measurements of reflection coefficient ($|S_{11}|$) and antenna gain are compared, whereas the simulated radiation pattern and cross-polarization results are shown due to a lack of pattern test equipment.

### 4.1. Reflection Coefficient ($|S_{11}|$)

The simulated and measured $|S_{11}|$ for the CCHA without HDL are below the $-10$ dB line over 1 GHz bandwidth, i.e., from 4.8 to 5.8 GHz. Additionally, Fig. 4 displays that the measured $|S_{11}|$ shifts to the left from the simulated $|S_{11}|$ in the case of CCHA with HDL by approximately 300 MHz. Interestingly, the measured $|S_{11}|$ amplitude is slightly better than the simulated results; however, it is clear that the trend is similar. The $|S_{11}|$ trends for the CCHA with HDL exhibit consistency between the simulated and measured results, with a 200 MHz decrease in bandwidth compared to the CCHA without HDL. The measurements indicate that the antenna's feed area, the change from the N-type connector to the air-line dielectric, and the connection of the feed pin to the connector have a significant impact on the results. To achieve the best return loss across the band, it is crucial to establish a proper contact between the connector receptacle and the feed pin. The measured $|S_{11}|$ results shown in Fig. 4 indicate a robust electrical continuity between the N-type connector's outer conductor and the metallic-coated sidewalls of the waveguide.

**Table 1.** Optimized design parameter values of CCHA and the HDL.

| Parameter | Value [mm] |
|---|---|
| Length of the CCHA ($L_1$) | 69 |
| Length of the waveguide ($L_2$) | 64 |
| Transition length ($L_3$) | 13 |
| Length of the HDL ($L_4$) | 150 |
| Top diameter of the CCHA ($D_1$) | 147 |
| Diameter of the waveguide ($D_2$) | 48.6 |
| Bottom horn diameter ($D_3$) | 57.3 |
| Outer top radius ($R$) | 78 |
| Inner top radius ($S$) | 70 |
| Outer base radius ($r$) | 20 |
| Inner base radius ($s$) | 12 |
| Wall thickness ($d$) | 8 |
| First corrugation spacing ($W_S$) | 9.2 |
| Last corrugation spacing ($W_{SN}$) | 9.2 |
| First corrugation height ($Sd1$) | 17.4 |
| Last corrugation height ($SdN$) | 10.7 |
| Corrugation thickness ($W_r$) | 2.3 |

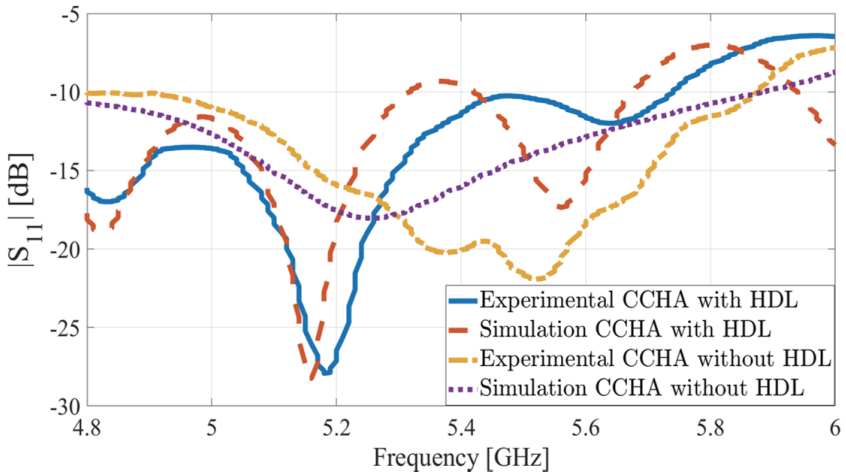


**Figure 4.** A simulation and measurement comparison of the CCHA $|S_{11}|$ with and without HDL.

### 4.2. Far-Field Gain

Figure 5 shows the experimental setup to measure the gain of the proposed 3D-printed CCHA using SH 1000 as the reference antenna and Keysight FieldFox VNA. Fig. 6 depicts a comparison of the antenna gain measurements for the proposed 3D-printed CCHA with and without HDL against the simulation results. The CCHA with HDL exhibits an average measured gain of 3 dBi higher than that of the standalone CCHA. The boresight gain measured for the antenna agrees well with the simulated gain, particularly for the CCHA with HDL. At 5.4 GHz design frequency, a gain enhancement of 2.5 dBi is achieved. The most significant gain enhancement, which reaches nearly 3.5 dBi, occurs at 6 GHz. The

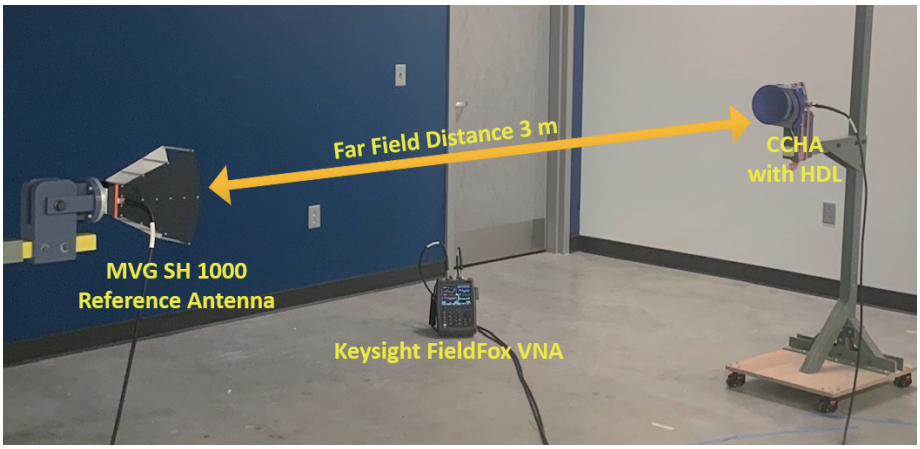


**Figure 5.** The measurement setup of the fabricated CCHA with HDL for the far-field gain.

measured results also exhibited an antenna gain lower than that of the simulation at low-operating frequencies, i.e., below 5.2 GHz, due to various factors such as air gaps and surface roughness. Further, the silver paint is lossy, and the impurities in the silver paint contribute to the antenna's low gain. The silver paint used had a resistivity of $5.3 \times 10^4\,\Omega \cdot \text{cm}$. Overall, a good agreement between measurements and simulations can be noticed after coating the CCHA prototype with at least two layers of silver paint.

Figure 7 displays the far-field radiation patterns for the co-polarization and cross-polarization at three frequencies of interest, which are 4.8, 5.4, and 6 GHz. At all three frequencies, the antenna co-polarization, which is gain, can be seen increasing with the addition of the HDL, and cross-polarization is decreasing. The increase in side lobe-level values can be seen as a concern; however, the value is still below −15 dB, which is ideal for most applications. Following placement of the HDL inside the CCHA, the electric field increased by 24% while the gain increased by 25% compared to the standalone CCHA. Table 2 compares the results for the antenna gain, electric field, side-lobes, and half-power beamwidth at

**Table 2.** Results summary for CCHA with and without HDL.

| Output Metric | CCHA without HDL | CCHA with HDL |
|---|---|---|
| $f_L = 4.8$ GHz | | |
| Gain [dBi] | 11 | 13.9 |
| Electric Field [dB (V/m)] | 24.4 | 32.3 |
| Side-Lobes [dB] | −23.8 | −17.7 |
| Half-Power Beamwidth | 58.8° | 22° |
| $f_C = 5.4$ GHz | | |
| Gain [dBi] | 13.3 | 15.6 |
| Electric Field [dB (V/m)] | 28.1 | 33.9 |
| Side-Lobes [dB] | −31.6 | −26.1 |
| Half-Power Beamwidth | 44.4° | 22° |
| $f_U = 6$ GHz | | |
| Gain [dBi] | 14.5 | 18 |
| Electric Field [dB (V/m)] | 29.2 | 35.1 |
| Side-Lobes [dB] | −28 | −29.5 |
| Half-Power Beamwidth | 37.6° | 22.3° |

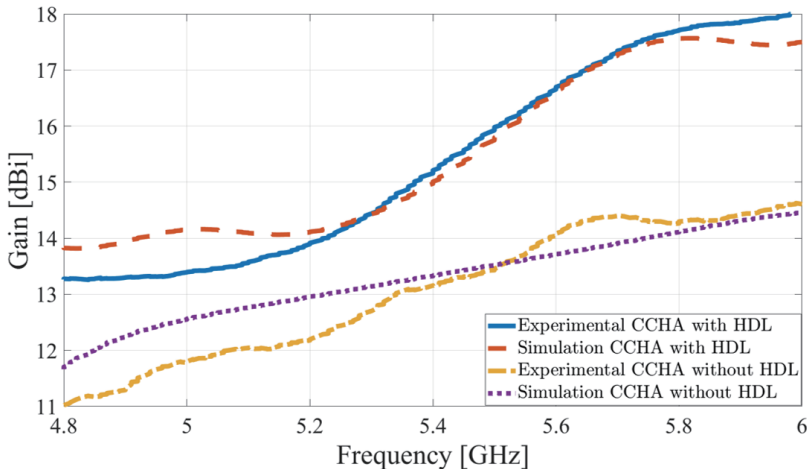


**Figure 6.** A simulation and measurement comparison of the CCHA gain with and without HDL.

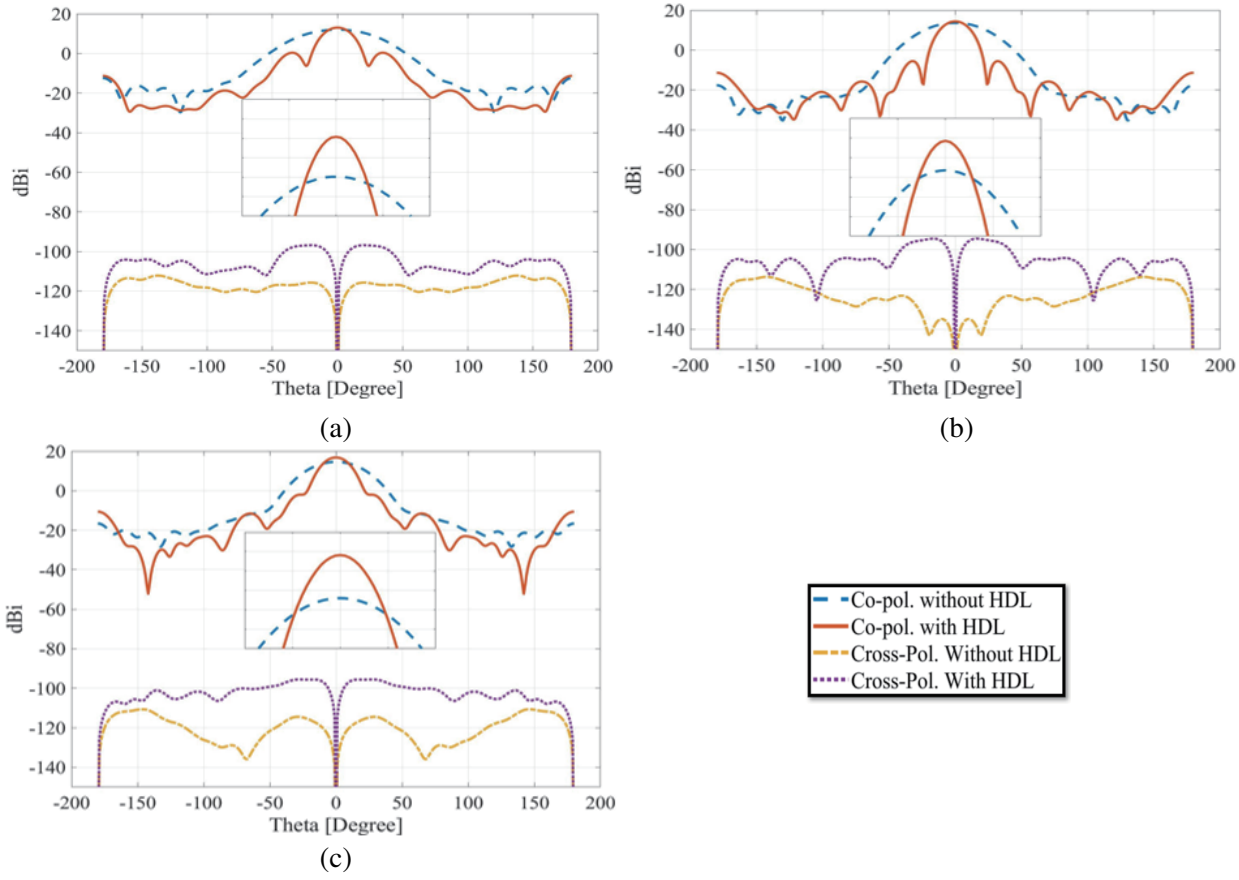


**Figure 7.** A simulation comparison of the CCHA co-polarization and cross-polarization with and without HDL at (a) 4.8 GHz, (b) 5.4 GHz, (c) 6 GHz.

the three frequencies of interest. When a time-varying electric field interacts with the polarized dipoles inside the HDL, it induces an EM field that produces another electric field, which enhances the incident field. An HDL with the optimal set of dimensions makes the CCHA more directive by combining the waves constructively. Such an improvement in the electric field intensity is desired from an antenna

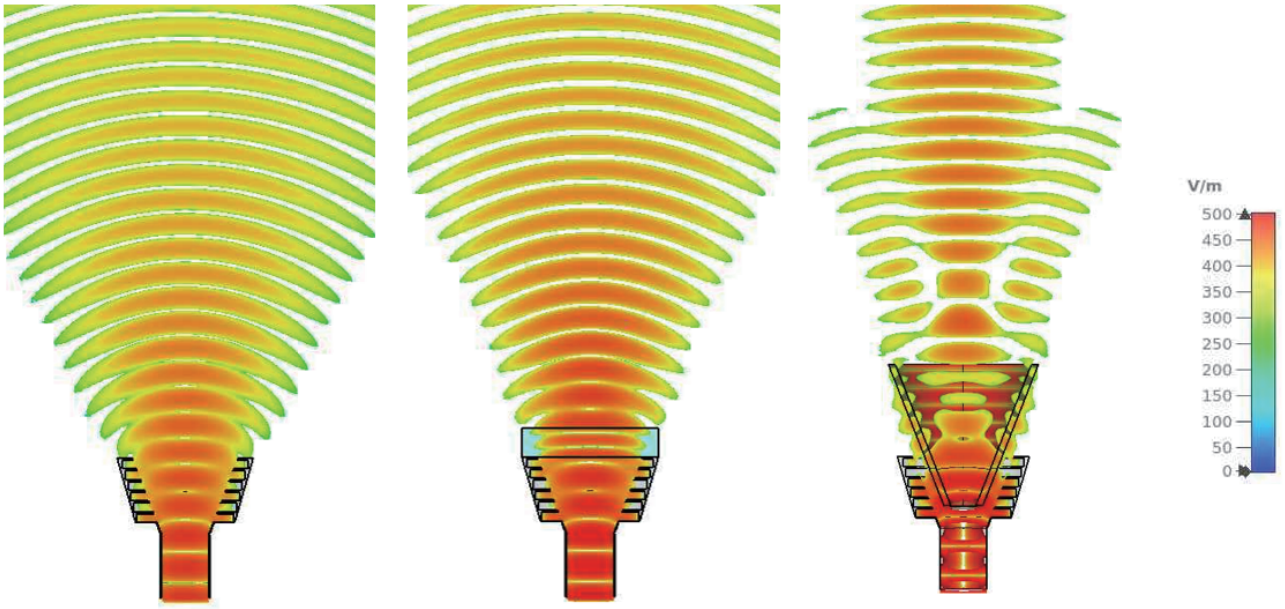


**Figure 8.** Conical corrugated horn antenna: (a) without HDL, (b) with dielectric solid lens, and (c) with HDL.

when it is excited by a fast sub-ns rise-time microwave source.

Figure 8(a) shows the view of a standalone CCHA, radiating electric field waves that propagate away from the CCHA in a wide beam at the aperture. Fig. 8(b) displays a side view of a CCHA with a traditional external loading that focuses the electric field on the boresight. In our work, the HDL is positioned inside the CCHA, as depicted in Fig. 8(c). The conductor and dielectric boundary create reflections that constructively add to the original signal, thereby increasing the electric field intensity at the far-field point. An EM wave striking the two dielectric interface generates reflected and transmitted waves. The amplitude and phase of these waves change from a normal incidence to an oblique incidence. The color bar indicates the electric field intensity, which increased significantly at the boresight when the HDL was introduced into the CCHA compared to the CCHA without loading and the CCHA with solid loading.

The proposed CCHA with HDL outperforms other lenses in Table 3 in terms of both required volume and mass, achieving a higher gain. The volume of HDL is much smaller than [7–11] resulting in a gain difference that is higher than all the other lenses. Furthermore, the weight of HDL is notably less than that of other lenses, indicating its suitability for applications that demand compact and lightweight lenses. The proposed lens also has the potential to fuel theoretical and application-oriented research.

**Table 3.** Comparison between HDL and other lenses.

| Method | $f_c$ [GHz] | Gain improvement [dBi] | Diagonal [cm] | Mass [g] | Volume to Gain [$cm^3$/dB] | Mass to Gain [g/dB] |
|---|---|---|---|---|---|---|
| [6] | 10 | 2.9 | $5.9\lambda_c$ | 737.6 | 227 | 245.8 |
| [7] | 5.5 | 1 | $1.5\lambda_c$ | 131.7 | 60 | 131.7 |
| [8] | 7.5 | 2.8 | $6.8\lambda_c$ | 3800 | 245 | 1357 |
| [9] | 11.5 | 4 | $12.5\lambda_c$ | 1001 | 113 | 250 |
| This Work | 5.4 | 3.5 | $2.8\lambda_c$ | 262.6 | 85 | 75 |

## 5. CONCLUSION

In this paper, we have proposed a novel wideband CCHA with an HDL with the objective of far-field gain improvement. The proposed HDL was optimized to achieve a higher far-field gain in a smaller form factor than horn antennas with traditional external lenses or simply horn antennas with long flare lengths. The optimized CCHA with an HDL obtained a nominal and peak gain improvement of 2 dBi and 3.5 dBi, respectively. The HDL reduces the volume by 40% and improves the electric field by 24% compared to commercial CCHA. Table 3 shows that the volume, weight, and maximum gain improvement of the loading have been enhanced over existing lenses. The gain measurements obtained with and without the loading are consistent with the simulation results, indicating a high level of agreement. To the best of our knowledge, this is the first time that a horn antenna's gain enhancement has been evaluated by simulating and measuring its performance using an HDL. The proposed loading design can be expanded to other horn antenna shapes and has potential applications in ground-penetrating radars, long-range communications, ground-to-UAV communications, and as a feed horn for dish reflectors.

## ACKNOWLEDGMENT

This work is supported in part by the School of Science and Engineering, UMKC, and in part by the Office of Naval Research under Grant No. N00014-22-1-2385.

## REFERENCES

1. Gupta, A., "A ridge-fed conical horn antenna for small satellites," *Master of Science Electrical Engineering*, The University of New Mexico Albuquerque, New Mexico, 2015.
2. Soares, P. A. G., P. Pinho, and C. A. Wuensche, "High performance corrugated horn antennas for CosmoGal satellite," *Procedia Technology*, Vol. 17, 667–673, 2014.
3. Chaudhary, S. V., D. Pujara, J. Gupta, and H. Pandya, "Corrugated horn antenna as mode transition for millimeter-wave plasma diagnostics system," *2019 IEEE Indian Conference on Antennas and Propagation (InCAP)*, 1–4, Ahmedabad, India, 2019.
4. Yadav, S. V. and A. Chittora, "A compact high power UWB TEM horn antenna," *2020 IEEE International Conference on Electronics, Computing and Communication Technologies (CONECCT)*, 1–3, Bangalore, India, 2020.
5. Li, Y., G. Lei, W. Junhong, D. Shan, C. Di, W. Jingxue, and L. Yang, "3-D printed high-gain wideband waveguide fed horn antenna arrays for millimeter-wave applications," *IEEE Transactions on Antennas and Propagation*, Vol. 67, No. 5, 2868–2877, 2019.
6. Belen, A., P. Mahouti, F. Güneş, and O. Tari, "Gain enhancement of a traditional horn antenna using 3D printed square-shaped multi-layer dielectric lens for X-band applications," *ACES Journal*, Vol. 36, No. 2, 132–138, 2021.
7. Asok, A. O., G. N. S J, and S. Dey, "Double ridge horn antenna with curved dielectric loading for microwave imaging applications," *2021 IEEE Indian Conference on Antennas and Propagation (InCAP)*, 167–170, Jaipur, Rajasthan, India, 2021.
8. Cao, Y., W. Menglong, S. Daoyuan, and S. Dan, "A novel miniaturized four-ridged horn antenna with enhanced gain," *International Journal of Antennas and Propagation*, Vol. 2021, 8143395, 2021.
9. Asok, A. O., G. N. S J, A. Tripathi, S. Chauhan, K. S. Kiran, and S. Dey, "Double ridge conical horn antenna with dielectric loading for microwave imaging of human breast," *2022 IEEE Wireless Antenna and Microwave Symposium (WAMS)*, 1–4, Rourkela, India, 2022.
10. Liu, X., Y. Chen, and Z. Nie, "Study on antenna gain for limited area of radiation aperture," *2019 IEEE International Conference on Computational Electromagnetics (ICCEM)*, 1–3, Shanghai, China, 2019.
11. Milligan, A. T., *Modern Antenna Design*, 285–335, John Wiley & Sons, Inc, 2005.

12. Ewing, P. D., "Approximation technique for determining gain and radiation pattern of the horn antenna," *Proceedings. IEEE Energy and Information Technologies in the Southeast*, 296–301, Columbia, SC, USA, 1989.
13. Baltzis, K. B., "Calculation of the half-power beamwidths of pyramidal horns with arbitrary gain and typical aperture phase error," *IEEE Antennas and Wireless Propagation Letters*, Vol. 9, 612–614, 2010.
14. Johnson, R. C., *Antenna Engineering Handbook*, 15–54, McGraw-Hill, 1993.
15. Balanis, A. C., *Antenna Theory: Analysis and Design*, 739–805, Wiley-Interscience, Hoboken, NJ, 2005.
16. Sahoo, S. K., M. Adhikary, A. Biswas, and M. J. Akhtar, "Multi-layer multi-dielectric lens loaded SIW horn antenna for Ku-band applications," *2021 15th European Conference on Antennas and Propagation (EuCAP)*, 1–5, Dusseldorf, Germany, 2021.
17. Gupta, R. C., S. Saxena, M. B. Mahajan, and R. Jyoti, "Design of dual-band multimode profiled smooth-walled horn antenna for satellite communication," *IEEE Antennas and Wireless Propagation Letters*, Vol. 9, 338–341, 2010.
18. Hu, N., S. Liu, J. Liu, L. Zhao, and W. Xie, "A novel ultra-wideband corrugated feed horn antenna for 5G application," *2022 IEEE Conference on Antenna Measurements and Applications (CAMA)*, 1–4, Guangzhou, China, 2022.
19. Bressner, T. A. H., M. N. Johansson, A. B. Smolders, and U. Johannsen, "Elliptical dual-polarized high gain horn antenna for cell partitioning in millimeter-wave mobile communications," *2020 50th European Microwave Conference (EuMC)*, 220–223, Utrecht, Netherlands, 2021.
20. MATLAB, The MathWorks Inc., https://www.mathworks.com/products/matlab.htm.
21. CST Studio Suite, Dassault Systems, https://www.3ds.com/productsservices/simulia/products/cst-studio-suite.
22. Jeffrey, A., *Handbook of Mathematical Formulas and Integrals*, 20–22, Academic Press, 1995.